Communications

Label-Free, Real-Time Monitoring of Biomass Processing with Stimulated Raman Scattering Microscopy**

Brian G. Saar, Yining Zeng, Christian W. Freudiger, Yu-San Liu, Michael E. Himmel, X. Sunney Xie,* and Shi-You Ding*

Research into alternative energy has experienced dramatic growth in recent years, which was motivated by both the environmental impact of current fossil fuels and the unstable and uncertain sources of oil and natural gas.[1] Under ideal conditions, currently unused plant materials, such as agricultural residues, forestry wastes, and energy crops, can be broken down by a series of chemical, enzymatic, and/or microbiological processes into ethanol or other biofuel sources. Biofuels offer an infinitely renewable source of carbon-neutral fuels that can be produced domestically and can make use of waste products from agricultural activity already taking place.[2] The major challenge to be overcome in the widespread adoption of many biofuels is that biomass is intrinsically recalcitrant,[3] making conversion into usable fuels inefficient. This, in turn, means that substantial energy is required to produce the current generation of biofuels, thus decreasing or eliminating their advantages as alternative sources of fuel.[4]

The two major chemical species of interest in the biomass conversion process are lignins and polysaccharides such as cellulose and hemicelluloses. Lignins are partly responsible for biomass recalcitrance,[5] but they may also have value as side products in the biorefineries of the future. Cellulose can be broken down to simple sugars, which can then be fermented to produce ethanol.[6] To address the recalcitrance problem presented by lignins, a thermochemical pretreatment process is necessary in current biomass conversion technology. This process uses oxidizing, acidic, or basic conditions along with elevated pressures and/or temperatures to remove or modify lignins and hemicelluloses, thereby enhancing the accessibility for the cellulase enzymes used in the breakdown of cellulose.[2,5,6] To optimize the overall conversion efficiency, a detailed understanding of the hydrolysis kinetics of polysaccharides and lignins is critical.

For this reason, analytical tools to study the biomass conversion process are needed. Herein, we demonstrate that stimulated Raman scattering (SRS) microscopy, a new imaging method, can offer new information on the biomass conversion processes. The ideal technique for studying the conversion process in situ should offer chemical specificity without exogenous labels, non-invasiveness, high spatial resolution, and real-time monitoring capability. Current analytical methods, such as gas chromatography–mass spectrometry, electron or scanning-probe microscopy, and fluorescence microscopy, cannot satisfy all of these requirements. Microscopy based on infrared absorption offers chemical specificity, but the spatial resolution is limited by the long infrared wavelengths, and penetration depth into aqueous plant samples is limited.[7] Raman microspectroscopy is widely used because it offers label-free chemical contrast with high resolution and chemical specificity.[8,9] However, the Raman scattering effect is weak, and long pixel dwell times (on the order of 0.1–1 s) are required for imaging plant materials.[9] This means that real-time imaging is challenging, as even a 256×256 pixel image would require almost two hours at 0.1 s/pixel. Consequently, the dynamic processes involved in the conversion cannot be followed at high spatiotemporal resolution.

Coherent Raman microscopy techniques solve many of these problems and offer label-free chemical imaging with high sensitivity and high spatial resolution. Coherent anti-Stokes Raman scattering (CARS) microscopy[10] is a technique that has been developed over the past ten years and applied to numerous problems of biological or biomedical relevance. However, CARS microscopy suffers from a non-resonant electronic background that can distort the chemical information of interest, making quantitative image interpretation challenging.[11]

Herein, we introduce stimulated Raman scattering (SRS)[12,13] as a tool to study biomass conversion. SRS

[*] B. G. Saar, Prof. X. S. Xie
Department of Chemistry and Chemical Biology
Harvard University, Cambridge, MA (USA)
Fax: (+1) 617-496-8709
E-mail: xie@chemistry.harvard.edu

Y. Zeng, Y. Liu, M. E. Himmel, S. Ding
Biosciences Center, National Renewable Energy Laboratory
Golden, CO (USA)
and
Bioenergy Science Center, Oak Ridge National Laboratory
Oak Ridge, TN (USA)
Fax: (+1) 303-384-7752
E-mail: shi.you.ding@nrel.gov

C. W. Freudiger
Department of Physics and
Department of Chemistry and Chemical Biology
Harvard University, Cambridge, MA (USA)

Supporting information for this article is available on the WWW under http://dx.doi.org/10.1002/anie.201000900.

microscopy offers chemical contrast based on the intrinsic Raman vibrational frequencies in the sample, similar to spontaneous Raman scattering, but it offers orders of magnitude larger signal levels.[13] SRS microscopy has been used to follow lipid uptake in living mammalian cells and drug diffusion into animal skin tissue, among other applications. Compared to the closely related CARS technique,[10] SRS offers the major advantages that it is free of the nonresonant background and linearly dependent on the analyte concentration. Furthermore, it offers an identical spectral response to spontaneous Raman scattering, allowing spectral assignment based on the wealth of Raman spectroscopy in the literature. In our implementation, SRS microscopy offers diffraction-limited spatial resolution (ca. 350 nm) and pixel dwell times of 50 µs. Thus a 256×256 pixel image requires only about 3 seconds with SRS, compared to about two hours with spontaneous Raman scattering.

In SRS microscopy, two near-infrared laser pulse trains are overlapped in time and space and focused onto the sample of interest by a laser scanning microscope with a high numerical aperture objective lens (Supporting Information, Figure S1). When the difference frequency between the two beams matches a vibrational resonance intrinsic to the sample, the vibrational transition rate is enhanced owing to stimulated excitation of vibrational transitions. This process is accompanied by energy transfer from the higher-frequency laser beam (called the "pump") to the lower frequency beam (called the "Stokes").[14] Importantly, this energy transfer only occurs when an intrinsic Raman-active vibrational mode at the difference frequency between the pump and Stokes beam appears in the sample. The signal is relatively small ($\Delta I/I < 10^{-3}$) and is buried in the noise of the laser system. For this reason, we employ a high-frequency (>1 MHz) amplitude modulation/lock-in detection procedure to improve the sensitivity of the technique (see Experimental Section) by eliminating the effect of low-frequency laser noise on images.[13]

Previous Raman spectroscopy studies have demonstrated that bands in the Raman spectrum of plant materials (Figure 1 a) are representative of lignin and cellulose.[8,9] The band at 1600 cm^{-1} corresponds to the aromatic stretching of lignin, and the bands from 1096–1122 cm^{-1} correspond to the C–C
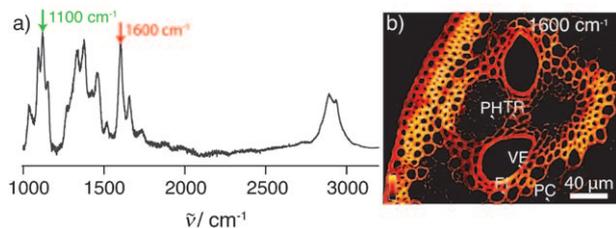

Figure 1. Raman spectroscopy and SRS imaging of corn stover. a) Raman spectrum of raw corn stover. The peak at 1600 cm^{-1} (red arrow) corresponds to the lignin distribution, and the peak at 1100 cm^{-1} (green arrow) corresponds to cellulose. b) SRS image of the vascular bundle including the edge of the stem in raw corn stover at 1600 cm^{-1}, showing the lignin distribution. Labeled structures are discussed in the text: parenchyma (PC), phloem (PH), vessel (VE), tracheid (TR), fiber (FI).

and C–O stretching in cellulose. By tuning the energy difference between the pump and Stokes laser beams into each of these bands, we imaged the distributions of the corresponding chemical species in fresh corn stover sections (Figure 1 b and Figure 2) using SRS. To validate the tech-
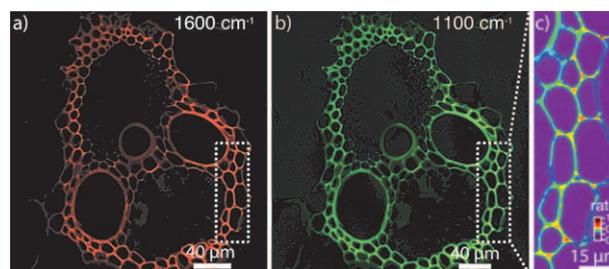

Figure 2. Imaging of lignin and cellulose with SRS microscopy. a) SRS image at 1600 cm^{-1} of another vascular bundle in the same sample as in Figure 1, showing the lignin distribution with a red intensity grade. b) SRS image of the same vascular bundle as in (a), showing the cellulose distribution at 1100 cm^{-1} with a green intensity grade. Both (a) and (b) are 1024×1024-pixel images obtained with a 50 µs pixel dwell time. These images can be acquired simultaneously using the two-color SRS instrument (see Experimental Section). c) Ratio of the lignin divided by the cellulose signal at higher magnification, obtained from the region surrounded by the dotted line in (a) and (b).

nique, a comparison of histological staining techniques and SRS microscopy was made in which the lignin channel is seen to correspond to the distribution of phloroglucinol, a lignin stain (Supporting Information, Figure S2). A similar correspondence can be seen between the cellulose channel and crystal violet stain for cellulose.

Using SRS imaging, we can observe the distribution of both lignin and cellulose simultaneously with subcellular resolution. Figure 1 b shows the intensities of SRS signals in different type of cells across maize stem. The images acquired at 1600 cm^{-1} represent lignin (Figure 2 a) and the image acquired at 1100 cm^{-1} represents cellulose (Figure 2 b). The parenchyma cells have large size and contain only primary cell walls, which show very weak lignin signal. Phloem cells also have low lignin content. The vessel, tracheid, and fiber cells are highly lignified (as much as seven times the signal of the phloem cells). The annular rings are the remains of the protoxylem secondary cell wall and show intermediate lignin content. Interestingly, in the large vessel cell (Figure 1 b), the lignin distribution appears to vary by more than a factor of three on different sides of the wall: the side adjacent to the tracheids appears to have less lignin. A possible explanation could be that these tracheids help control the lateral distribution of water from vessels across the stem.

The cellulose content is more evenly distributed than the lignin. Parenchyma and phloem cells show more contrast in the cellulose channel compared to the lignin channel. A higher-magnification ratio image (Figure 2 c) can be used to show the ratio between lignin and cellulose signals, and was obtained by dividing the images in Figure 2 a and b (see also the Supporting Information). It allows relative quantitation[20] to visualize the areas of high and low lignin/cellulose ratio.

The image demonstrates that lignin content is particularly high in the cell corners; this result is similar to previous results from Raman imaging, and is consistent with the hypothesis that lignification occurs initially in the cell corners and then follows the path from the primary cell wall to the secondary cell walls (from the S1 to the S3 layer).[15] Our observation that the lumen side of the cell wall (the S3 layer) has the lowest lignin content and the highest cellulose content also supports this. Such observations are difficult to make with CARS because the nonresonant background of that technique can vary spatially, making the chemical information of interest difficult to separate from the background image.

The high spatiotemporal resolution of SRS microscopy allows us to follow a delignification reaction using the acid chlorite method[16] in real time in three dimensions with submicrometer resolution. This method, which is widely used in the paper and wood industry to remove lignin, uses sodium chlorite ($NaClO_2$) and acid to generate chlorine dioxide, chlorine, and chlorate as delignification reagents. It is known that the acid chlorite treatment removes lignin with high selectivity for the first 60% of the lignin removed, after which a small amount of cellulose is also hydrolyzed.[16] Nonetheless, it is perhaps the best example of a process for studying "pure" delignification by chemical means.[16]

To study this process, we positioned a 150-micrometer-thick slice of corn stover stem at the focus of the SRS microscope (see Experimental Section). We chose to focus on a vascular bundle, as this structure contains a number of different cell types. We simultaneously acquired lignin and cellulose channels at about 8 s/image. The sample was contained within a flow cell so that the initial image could be acquired and then the treatment reagents could be flowed in to begin the digestion. The time course of the reaction was less than one hour under the conditions that we used, which is faster than the acquisition time for a single image in spontaneous Raman scattering.

Figure 3 a–d shows images of the lignin and cellulose channels before and after the time course of the reaction. The integrated intensity demonstrates the selectivity of the reaction: The lignin signal decreases by more than eightfold, whilst the cellulose signal remains constant to within the noise of the measurement. By removing the drift from the image (see the Supporting Information), it was possible to then extract the time trace of the reaction at each point in the sample with submicrometer resolution. This time trace could then be fitted with a single exponential to determine an effective reaction rate at each location, which is plotted as a

heat map in Figure 3 e (with typical time constants on the order of hundreds of seconds). Representative traces from different locations in the sample are shown in Figure 3 f–i. We observed no decay in background, rapid decay in the phloem, and slower decay in the fiber and vessel cells.

Reaction rates are heterogeneous even on the micrometer scale, and the limited spatial and temporal resolution of spontaneous Raman scattering are insufficient to capture this information. For example, the region of the phloem, which has lower lignin content than the surrounding fibers, also manifests the most rapid bleaching kinetics of lignin. Furthermore, the bleaching is more rapid on the edges of the plant tissue than at the center of the thicker cell wall, possibly because the edges are more exposed to the surrounding solvent. There are significant variations in the initial lignin content (more than a factor of four differences in signal level) in the parenchyma as compared to other thick-walled cells (fibers, tracheids, and vessels). Nonetheless, they manifest quite similar bleaching kinetics, suggesting that the accessibility of the lignin to the bleaching reagents is similar. We verified that the observed kinetics are not due to photobleaching by performing imaging for a similar time period on a sample that was not chemically treated, in which case the sample was unchanged (Supporting Information, Figure S3).

In summary, the high spatiotemporal resolution afforded by SRS microscopy, together with the label-free chemical contrast, offers a unique tool for studying the degradation of biomass in real time without the use of labels. Compared to traditional spontaneous Raman scattering, the acquisition speed is enhanced by more than three orders of magnitude without sacrificing spatial resolution or image quality. Furthermore, SRS is intrinsically immune to background auto-
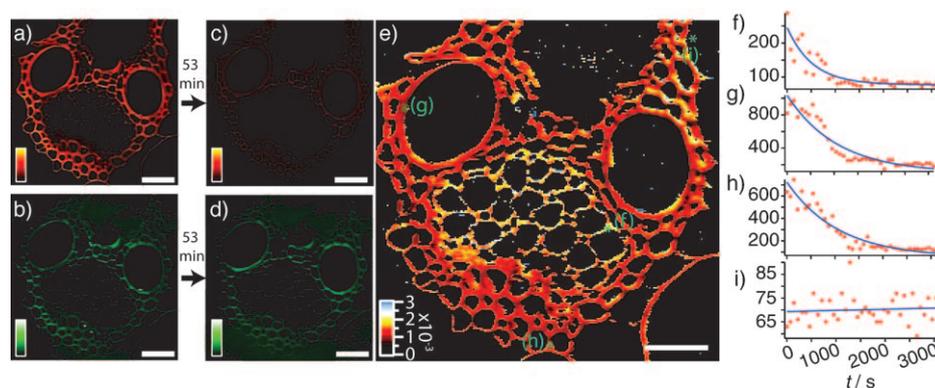

Figure 3. Real-time SRS imaging of a delignification reaction in corn stover. All images were taken in the same vascular bundle. a) Lignin signal at 1600 cm^{-1} before the start of the reaction. b) The cellulose signal at 1100 cm^{-1} before the start of the reaction. c) Lignin signal after a 53 min time course of acid chlorite treatment, showing significant reduction (more than eightfold) compared to (a). d) Cellulose signal after treatment, which remains roughly the same as in (b). e) False-color heat map of the reaction rate constant obtained by fitting the time series of the lignin decay in the reaction to a single exponential. The initial and final points are shown in images (a) and (c). The rate-constant [s^{-1}] color scale is shown in the bottom left corner. f–i) Representative time traces (red dots) and single-exponential fits (blue lines) from four locations labeled as green spots in (e), representing a phloem element (f), vessel (g), fiber (h), and background with no plant cell wall (i) in the corn stover sample. The image in part (e) consists of 256×256 pixels, each of which has an associated single exponential decay fit to obtain the rate constant. Acquisition time: about 8 s/frame; spatial resolution: 900 nm (limited by the sampling of the images). Scale bars: 40 micrometers.

fluorescence that can contaminate spontaneous Raman signals from plant materials. Technical developments, particularly in the area of laser sources, will likely have a dramatic impact on the cost and complexity of a system like this as robust, permanently aligned optical-fiber-based light sources become widely used for multiphoton microscopy.[17–19]

Because the SRS signal is linearly dependent on chemical concentration and has no background offset, the image contrast can be interpreted according to the Raman literature. Recording "chemical movies" of this chemical reaction in progress allows us to visualize the spatial variation of the reaction rate to understand which parts of the plant are degraded most efficiently by the treatment process. This technique can be readily applied under a variety of experimental conditions (such as temperature, pressure, and pH) to understand the pretreatment reaction, and it could also be useful for studying the enzymatic breakdown of cellulose or for in vivo imaging of lignification and cellulose biosynthesis in plant cell-wall development.

Experimental Section

Field-dried Mo17 maize was harvested in Madison, WI in fall of 2003. The samples were sliced to 150 μm thickness by a rotary microtome and sandwiched between cover slips using double-sided tape. To monitor the chemical bleaching process, the sample was placed in a flow channel between the two cover slips. Initially, samples were imaged in phosphate-buffered saline. To initiate the delignification reaction, a solution of 0.1M HCl (aq) and 10% $NaClO_2$ was flowed into the channel. SRS microscopy was performed on the samples using a two-color instrument similar to one described previously.[13] A high-power picosecond Nd:YVO$_4$ oscillator (picoTrain, High Q Laser, Austria) producing a 76 MHz train of 7 ps pulses at 1064 nm was used as the Stokes beam, and was amplitude-modulated at 10 MHz. A portion of the same 1064 nm laser beam was also frequency-doubled and split to pump two synchronously pumped optical parametric oscillators (Levante Emerald, APE GmbH, Germany), each of which provides an independently tunable pump beam. The three beams were combined in space and time using dichroic mirrors and mechanical delay stages (Supporting Information, Figure S1). A laser scanning microscope (BX62WI/FV300, Olympus, Japan) is used to scan the focal spot of the three beams over the sample in the flow chamber, and the transmitted pump light is separated into individual channels and detected by large area photodiodes. Each channel is demodulated by a lock-in amplifier (SR844, Stanford Research Systems, USA), which provides the SRS signal corresponding to lignin (when the pump wavelength is about 910 nm) or cellulose (when the pump wavelength is about 953 nm). Movies of the delignification process were acquired using the data-acquisition software of the microscope (FV5, Olympus, Japan), and processed using custom-written image correlation software to remove the effects of sample drift on the kinetic maps.

[1] S. Herrera, *Nat. Biotechnol.* **2006**, *24*, 755.
[2] P. Kumar, D. M. Barrett, M. J. Delwiche, P. Stroeve, *Ind. Eng. Chem. Res.* **2009**, *48*, 3713.
[3] N. Mosier, C. Wyman, B. Dale, R. Elander, Y. Y. Lee, M. Holtzapple, M. Ladisch, *Bioresour. Technol.* **2005**, *96*, 673.
[4] D. Pimentel, T. W. Patzek, *Nat. Resour. Res.* **2005**, *14*, 65.
[5] M. E. Himmel, S.-Y. Ding, D. K. Johnson, W. S. Adney, M. R. Nimlos, J. W. Brady, T. D. Foust, *Science* **2007**, *315*, 804.
[6] D. M. Mousdale, *Biofuels: Biotechnology, Chemistry, and Sustainable Development*, CRC, Boca Raton, FL, **2008**.
[7] N. Jamin, P. Dumas, J. Moncuit, W.-H. Fridman, J.-L. Teillaud, G. L. Carr, G. P. Williams, *Proc. Natl. Acad. Sci. USA* **1998**, *95*, 4837.
[8] U. Agarwal, *Planta* **2006**, *224*, 1141.
[9] a) N. Gierlinger, M. Schwanninger, *Plant Physiol.* **2006**, *140*, 1246; b) M. Schmidt, A. M. Schwartzberg, P. N. Perera, A. Weber-Bargioni, A. Carroll, P. Sarkar, E. Bosneaga, J. J. Urban, J. Song, M. Y. Balakshin, E. A. Capanema, M. Auer, P. D. Adams, V. L. Chiang, P. James Schuck. *Planta* **2009**, *230*, 589.
[10] C. L. Evans, X. S. Xie, *Annu. Rev. Anal. Chem.* **2008**, *1*, 883.
[11] L. Li, H. Wang, J.-X. Cheng, *Biophys. J.* **2005**, *89*, 3480.
[12] E. Ploetz, S. Laimgruber, S. Berner, W. Zinth, P. Gilch, *Appl. Phys. B* **2007**, *87*, 389.
[13] C. W. Freudiger, W. Min, B. G. Saar, S. Lu, G. R. Holtom, C. He, J. C. Tsai, J. X. Kang, X. S. Xie, *Science* **2008**, *322*, 1857.
[14] M. D. Levenson, S. S. Kano, *Introduction to Nonlinear Laser Spectroscopy*, Revised ed., Academic Press, Inc., San Diego, CA, **1988**.
[15] L. B. Davin, A. M. Patten, M. Jourdes, N. G. Lewis, in *Biomass Recalcitrance* (Ed.: M. Himmel), Wiley-Blackwell, Oxford, UK, **2008**.
[16] P. A. Ahlgren, D. A. I. Goring, *Can. J. Chem.* **1971**, *49*, 1272.
[17] E. R. Andresen, C. K. Nielsen, J. Thøgersen, S. R. Keiding, *Opt. Express* **2007**, *15*, 4848.
[18] K. Kieu, B. G. Saar, G. R. Holtom, X. S. Xie, F. W. Wise, *Opt. Lett.* **2009**, *34*, 2051.
[19] G. n. Krauss, T. Hanke, A. Sell, D. Träutlein, A. Leitenstorfer, R. Selm, M. Winterhalder, A. Zumbusch, *Opt. Lett.* **2009**, *34*, 2847.
[20] R. L. McCreery, *Raman Spectroscopy for Chemical Analysis*, Wiley, New York, **2000**.